

# Universal Fermi-surface anisotropy renormalization for interacting Dirac fermions with long-range interactions

Jia Ning Leaw,<sup>1</sup> Ho-Kin Tang,<sup>1</sup> Maxim Trushin,<sup>2</sup> Fakher F. Assaad,<sup>3</sup> Sankar Das Sarma,<sup>4</sup> and Shaffique Adam<sup>1,5,\*</sup>

<sup>1</sup>*Department of Physics and Centre for Advanced 2D Materials,  
National University of Singapore, 2 Science Drive 3, 117551, Singapore*

<sup>2</sup>*Centre for Advanced 2D Materials, National University of Singapore, 6 Science Drive 2, Singapore 117546*

<sup>3</sup>*Institut für Theoretische Physik und Astrophysik,  
Universität Würzburg, Am Hubland, D-97074 Würzburg, Germany.*

<sup>4</sup>*Condensed Matter Theory Center and Joint Quantum Institute,  
Department of Physics, University of Maryland, College Park, Maryland 20742, USA*

<sup>5</sup>*Yale-NUS College, 16 College Avenue West, 138614, Singapore*

Recent experimental<sup>1</sup> and numerical<sup>2</sup> evidence suggest an intriguing universal relationship between the Fermi surface anisotropy of the non-interacting parent two-dimensional electron gas and the strongly correlated composite Fermi liquid formed in a strong magnetic field close to half-filling. Inspired by these observations, we explore more generally the question of anisotropy renormalization in interacting 2D Fermi systems. Using a recently developed<sup>3</sup> non-perturbative and numerically-exact projective quantum Monte Carlo simulation as well as other numerical and analytic techniques, only for Dirac fermions with long-range Coulomb interactions do we find a universal square-root decrease of the Fermi-surface anisotropy. For the  $\nu = 1/2$  composite Fermi liquid, this result is surprising since a Dirac fermion ground state<sup>4</sup> was only recently proposed as an alternative to the usual HLR state<sup>5</sup>. The importance of the long-range interaction, expected for Dirac systems<sup>6</sup>, is also consistent with recent transport measurements<sup>7</sup>. Our proposed universality can be tested in several anisotropic Dirac materials including graphene, topological insulators<sup>8</sup> and organic conductors<sup>9</sup>.

A plethora of quantum Hall ground states are observed when the two-dimensional electron gas is placed in a strong magnetic field. Unique among these states is when the system is tuned to half-filling; here rather than observing an insulator as is typical, instead a metallic state is observed. This compressible phase called a “composite Fermi liquid” is believed to emerge because at the mean field level, the magnetic flux attached to each composite

fermion exactly cancels the external magnetic field<sup>10,11</sup>. The Fermi surface properties of this metallic state have long been explored. A very recent experiment at Princeton measured how the anisotropy of this strongly correlated Fermi surface along the high-symmetry axis (parameterized by  $\eta$ , defined below) was related to that of the original Fermi surface  $\eta_0$  of the non-interacting electrons in the absence of an external magnetic field<sup>1</sup>. Before performing the experiment, they surveyed leading theorists on what they expected to observe, obtaining a range of answers: since the composite Fermi liquid was a universal strongly correlated ground state, in which the kinetic energy of the non-interacting bands were quenched, some expected no Fermi surface anisotropy in the composite Fermi liquid; others expected the state to have the same anisotropy as the non-interacting bands from which the state emerged. Remarkably, the experiment observed that  $\eta = \sqrt{\eta_0}$  i.e. the interacting state was always more isotropic and universally so.

This experiment motivated us to ask a more fundamental question. What is the relationship between the Fermi surface anisotropy of an interacting Fermi liquid given a fixed anisotropy of the non-interacting bands i.e. we are interested not only in the effective composite Fermi liquid at  $\nu = 1/2$ , but the interacting 2D Fermi liquid in general. To illustrate that the answer is not obvious consider the following. One might expect that interactions enhance the anisotropy. Anisotropy can be thought of as broken rotational symmetry, and it was predicted long ago that the exchange interaction can enhance the splitting between broken symmetry states<sup>12</sup>. In the quantum Hall context, interaction-enhanced Zeeman splitting has been seen experimentally for the graphene integer quantum Hall effect<sup>13</sup> and more recently, an interaction-induced spontaneous symmetry breaking of nematic phases<sup>14</sup>.

---

\* shaffique.adam@yale-nus.edu.sg

In other contexts, interactions wash away non-universal particularities of the non-interacting model flowing to a universal interacting fixed point (the universal  $\nu = 1/3$  Laughlin state observed in different parent materials and with different confining potentials leading to different effective interactions, is but one example). Experimentally, the observed sequence of fractional quantum Hall plateaus in graphene suggest that the strongly interacting ground state partially restores the spin and valley splitting of the non-interacting system<sup>15</sup>. For the specific case of  $\nu = 1/2$ , using a Gaussian approximation for the electron-electron interactions, Ref. 16 found analytically that interactions always make the composite Fermi liquid more isotropic, but in a non-universal way where  $\eta/\eta_0$  could take on values between 0 and 1 depending on the length scale of the Gaussian. Other calculations in specific models<sup>17,18</sup> suggest no change in the Fermi surface anisotropy; while yet others show a non-universal decrease in anisotropy<sup>19,20</sup>.

We are not the first to ask the question about the many-body renormalization of anisotropic Fermi surfaces. Back in 1960, Kohn and Luttinger<sup>21</sup> argued that the standard diagrammatic perturbation theory to account for electron-electron interactions failed when considering anisotropic Fermi surfaces. Moreover, the effect of correlations was understood to be non-universal where the anisotropy renormalization depends on material specific parameters like the effective mass, carrier density and dielectric substrate. Below we reproduce the leading order term for “Schrödinger electrons” where the bare band dispersion is of the usual parabolic energy form to illustrate how this non-universality arises for generic band structures. However, and remarkably, we find that for Dirac fermions (e.g. graphene) with bare Fermi velocity anisotropy, in the presence of a long-range Coulomb interaction, there is a universal relationship  $\eta = \sqrt{\eta_0}$  that does not depend on any of the material-specific parameters mentioned above. We emphasize that the long-range nature of the Coulomb potential is essential: our analytical and numerical results also suggest that Dirac fermions with only contact interactions retain the anisotropy of the original non-interacting system. We find that the chirality of the Dirac bands and the long-range interaction are both necessary to obtain the square-root anisotropy.

In the presence of Coulomb interactions, the properties of correlated Dirac fermions are governed by two very different fixed points<sup>3</sup>. There is a stable “weak-coupling” fixed point determined entirely by the long-range Coulomb tail, which flows at low energies to a non-

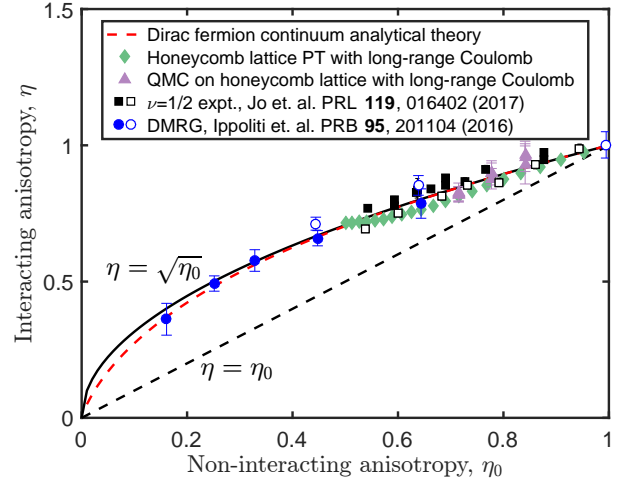


FIG. 1. Universal decrease of Fermi-velocity anisotropy for long-range interacting Dirac fermions. Analytical perturbation theory and Hartree-Fock results for Dirac fermions (red dashed line) show a square-root decrease of the Fermi velocity anisotropy. Lattice perturbation theory on the honeycomb lattice (green diamonds) and the non-perturbative projective Quantum Monte Carlo (purple triangles) are consistent with this square-root behaviour. Also shown are recent experiments (black squares) and density matrix renormalization group calculations (blue circles) for the  $\nu = 1/2$  quantum Hall state. We find that both the chirality of the Dirac bands and a long-range interaction potential are necessary for this universal decrease in anisotropy.

interacting Lorenz invariant theory (where the electron Fermi velocity is equal to the speed of the light). Then there is also an unstable “strong-coupling” Gross-Neveu fixed point controlled by the contact part of the Coulomb interaction and associated with the transition to a Mott insulating antiferromagnet at half-filling. While ultimately unstable, the proximity to the strong coupling fixed point is largely responsible for most experimentally observable properties of Dirac fermions. Paradoxically, the closer to the “strong-coupling” fixed point the flow of Dirac fermion under interactions starts, the more it behaves like the non-interacting theory (with typical Fermi velocities about two or three orders of magnitude slower than the speed of light)<sup>3</sup>. The dichotomy between the long-range and contact part of the Coulomb potential for Dirac fermions was also discussed in Ref. 22. Since this particular velocity renormalization influences all points on the Fermi surface equally, it drops out when calculating the anisotropy renormalization that we are concerned with here.

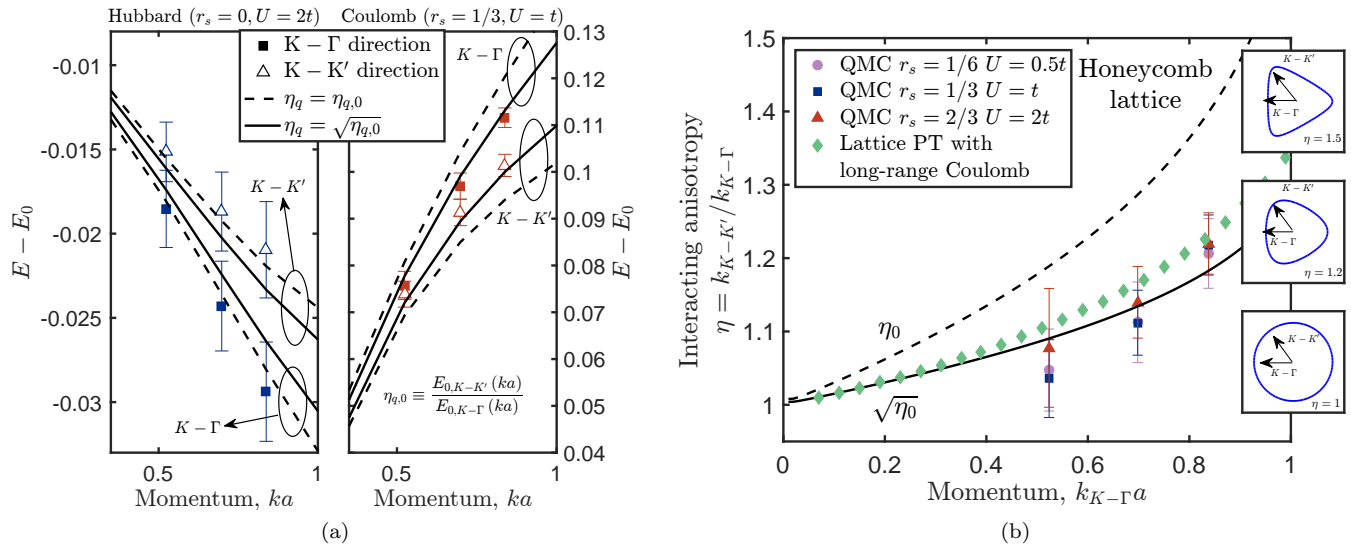


FIG. 2. Non-perturbative quantum Monte Carlo simulations on a honeycomb lattice also show universal square-root anisotropy renormalization with long-range Coulomb interactions, but not for Hubbard interactions. (a) QMC data with onsite Hubbard interaction (left panel) and long-range Coulomb interaction (right panel). The energy renormalization  $E - E_0$  of the quasiparticle is obtained for  $K - \Gamma$  direction (squares) and  $K - K'$  direction (triangles). Solid lines indicate what one would expect for a square-root renormalization, while dashed lines show no anisotropy renormalization. (b) The interacting theory anisotropy as a function of momentum away from the Dirac point. The honeycomb lattice is isotropic as momentum vanishes but becomes more anisotropic at larger momentum. Both the non-perturbative QMC and the lattice perturbation theory show a clear square-root anisotropy renormalization for long-range Coulomb interactions.

To build some intuition into our results, we begin by considering the Hartree-Fock approximation and first-order perturbation theory (for the case we consider, both these considerations give identical results, see Methods section below). This is the leading-order many-body result as expanded directly in the bare interaction. We first observe that for Dirac fermions, the contact interaction does not renormalize the Fermi velocity (see e.g. Ref. 23 and Methods section). For the long-range Coulomb interaction, the dominant contribution comes from the filled hole bands. Although the Fermi surface is vanishing at the Dirac point, the Fermi surface anisotropy is still well-defined. By first setting a finite Fermi level (defined by a Fermi momentum  $k_F$ ) and then taking the limit  $k_F \rightarrow 0$ , the Fermi surface anisotropy converges to the Fermi velocity anisotropy  $\eta_0 = v_x/v_y$ , where the subscript denotes that this is the non-interacting system. When the 2D Coulomb interaction is turned on, the effective single particle energy is corrected by the exchange correlation, which within the Hartree-Fock approximation is

given by<sup>24</sup>

$$E^{HF}(\mathbf{k}) = - \int_{\Omega} \frac{d^2\mathbf{k}'}{(2\pi)^2} \frac{2\pi e^2}{\epsilon|\mathbf{k} - \mathbf{k}'|} \sin^2\left(\frac{\varphi_{\mathbf{k}} - \varphi'_{\mathbf{k}}}{2}\right), \quad (1)$$

where  $e$  is the electron charge,  $\epsilon$  is the dielectric relative permittivity, and  $\tan \varphi_{\mathbf{k}} = (v_y k_y)/(v_x k_x)$ . The  $\varphi_{\mathbf{k}}$ -dependent factor accounts for the chirality of the Dirac fermions. Calculating the anisotropy (see Methods), we find

$$\eta = \frac{E(1 - \eta_0^2) - K(1 - \eta_0^2)}{K(1 - \eta_0^{-2}) - E(1 - \eta_0^{-2})} \approx \sqrt{\eta_0}. \quad (2)$$

Here  $K(z)$  and  $E(z)$  are the complete elliptic integrals of the first and second kind respectively. This analytic result is shown as the red curve in Fig. 1, and it is remarkably close to the line  $\eta = \sqrt{\eta_0}$ . Since within Hartree-Fock and first-order perturbation theory the exchange energy contribution dominates over the non-interacting contribution, it is not surprising that the result is universal, nonetheless this behavior is unique (see Methods) to Dirac fermions in two-dimensions with a long-range Coulomb interaction. We emphasize

that chirality is essential for our result. The chiral eigenfunctions of the Dirac fermions are invariant to the Hartree-Fock interaction and neglecting these, or even changing the winding number from 1 breaks the universality. By contrast, particle-hole symmetry breaking terms do not couple to the chirality and preserve the universality (see Methods for details).

While the perturbative approach is useful to understand qualitatively how the universality arises in the Dirac system, here we use a non-perturbative, numerically exact projective quantum Monte Carlo simulation appropriate for the strongly correlated nature of the ground state. We use a honeycomb lattice with nearest neighbor hopping (as appropriate, e.g., for graphene) and at half-filling there is no fermion sign problem. We are able to separately tune the short-range or Hubbard  $U$  and long-range tail  $r_s/r$  components of the Coulomb interaction (see Methods). The non-interacting system contains Dirac cones at the high-symmetry  $K$ ,  $K'$  points in the Brillouin zone that are isotropic in the low-energy limit, but have trigonal warping away from the Dirac point naturally providing an anisotropic Fermi surface, whose renormalization with interactions we can explore. Appropriate for the three-fold symmetry, we define  $\eta_q$  as the ratio of the energy deviation  $(E - E_0)_{K-K'}/(E - E_0)_{K-\Gamma}$  at a fixed momentum, where  $K - K'$  and  $K - \Gamma$  are the principal directions.

Our results are obtained from a finite-size scaling of the numerical data on lattice sizes up to  $24 \times 24$  unit cells. The left panel of Fig. 2a shows a typical case where short-range interactions are dominant ( $r_s = 0; U = 2t$ ). In this case the correlation induced velocity renormalization is very small, and the data are consistent with no renormalization of the anisotropy,  $\eta_q = \eta_0$  within the error bars. The right panel is typical for when the long-range tail dominates ( $r_s = 1/3, U = t$ ). The data shows that strongly correlated Dirac fermions with long-range Coulomb interactions have the universal  $\eta_q = \sqrt{\eta_{q,0}}$ . To complement the quantum Monte Carlo, we calculate first order perturbation theory on the honeycomb lattice, allowing us to go to much bigger system sizes ( $1500 \times 1500$  unit cells), showing again good agreement with the square-root renormalization of the anisotropy (see Methods for details). The various numerical and analytical approaches all confirm that the long-range Coulomb potential gives a universal square-root suppression of the bare anisotropy for interacting Dirac fermions, reminiscent of the experimental finding at the half-filled Landau level in Ref. 1.

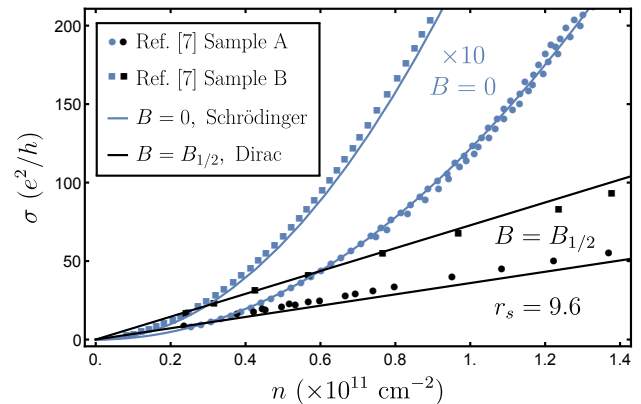


FIG. 3. The bare electron and composite fermion conductivities,  $\sigma$ , vs. fermion concentration,  $n$ , obtained for a given sample at zero magnetic field ( $B = 0$ ) and near half-filling ( $B = B_{1/2}$ ). The circles and squares are the experimental data by Pan et al.<sup>7</sup> for two different samples. The zero-field data shows a quadratic trend fitted by the Boltzmann conductivity for Schrödinger fermions with impurity concentrations  $n_i = 1.9 \times 10^7 \text{ cm}^{-2}$  and  $9.6 \times 10^6 \text{ cm}^{-2}$  for samples A and B respectively. The conductivity at half-filling for both samples is then obtained by the Boltzmann conductivity for Dirac fermions assuming a single Fermi velocity  $v = \sqrt{v_x v_y} = 1.8 \times 10^6 \text{ cm/s}$ .

A natural interesting question is whether this is a mere coincidence or is an indicator for the predicted emergent Dirac fermion nature of the half-filled Landau level. While answering this question definitively is well beyond the scope of the current work, which is entirely on the many-body renormalization of bare anisotropy in zero-field interacting 2D Dirac and Schrödinger systems, we mention one more tantalizing experimental finding in this context by Pan et al.<sup>7</sup> who established that the half-filled Landau level conductivity in high-mobility modulation-doped 2D structures manifests a linear-in-carrier density dependence (similar to that observed in graphene<sup>25</sup>) in contrast to the expected quadratic density dependence observed and predicted in the corresponding zero-field 2D conductivity of the usual Schrödinger system<sup>26</sup>. If our speculations about a possible connection between our result and the emergent Dirac nature of the composite fermion liquid at half-filling are correct, then it also follows that the long-range nature of Coulomb interaction is an essential part of the physics here since we only find the square-root suppression of the bare anisotropy for long-range Coulomb interaction and not for the short-range contact interaction.

Shown in Fig. 3 is the conductivity for two of the samples reported in Ref. 7 both at  $B = 0$  (blue data) and close to half-filling (black data). For unscreened long-range interactions, the conductivity  $\sigma \sim (e^2/h)(n/n_i)(1/r_s^2)$ , where  $r_s = e^2/(\epsilon\hbar\sqrt{v_x v_y})$  is density independent for Dirac fermions but scales as  $\sqrt{n}$  for Schrödinger fermions. Assuming that for each sample the impurity concentration  $n_i$  is the same both at  $B = 0$  and at half-filling, this allows us to fit for the conductivity of

the composite Fermi liquid with a single Dirac Fermi velocity  $v = \sqrt{v_x v_y} = 1.8 \times 10^6$  cm/s. This corresponds to  $r_s \sim 10$ , which is more than an order of magnitude more strongly interacting than most other condensed matter realizations of Dirac fermions. Finally, we encourage experimentalists working with graphene, surface states of topological insulators or layered organic conductors (all of which support anisotropic bare Dirac fermions) to look for our proposed universal many-body renormalization induced suppression of the anisotropy.

- 
- <sup>1</sup> Jo, I. *et al.* Transference of fermi contour anisotropy to composite fermions. *Phys. Rev. Lett.* **119**, 016402 (2017). URL <https://link.aps.org/doi/10.1103/PhysRevLett.119.016402>.
- <sup>2</sup> Ippoliti, M., Geraedts, S. D. & Bhatt, R. N. Numerical study of anisotropy in a composite fermi liquid. *Phys. Rev. B* **95**, 201104 (2017). URL <https://link.aps.org/doi/10.1103/PhysRevB.95.201104>.
- <sup>3</sup> Tang, H. K. *et al.* The role of electron-electron interactions in two-dimensional Dirac fermions. *Science* **361**, 570–574 (2018). URL <http://science.sciencemag.org/content/361/6402/570>. 1808.03648.
- <sup>4</sup> Son, D. T. Is the composite fermion a dirac particle? *Phys. Rev. X* **5**, 031027 (2015). URL <https://link.aps.org/doi/10.1103/PhysRevX.5.031027>.
- <sup>5</sup> Halperin, B. I., Lee, P. A. & Read, N. Theory of the half-filled landau level. *Phys. Rev. B* **47**, 7312–7343 (1993). URL <https://link.aps.org/doi/10.1103/PhysRevB.47.7312>.
- <sup>6</sup> Adam, S., Hwang, E. H., Galitski, V. & Sarma, S. D. A self-consistent theory for graphene transport. *Proc. Natl. Acad. Sci.* **104**, 18392–18397 (2007). URL <http://arxiv.org/abs/0705.1540> <http://dx.doi.org/10.1073/pnas.0704772104>. 0705.1540.
- <sup>7</sup> Pan, W. *et al.* Berry phase and anomalous transport of the composite fermions at the half-filled landau level. *Nature Physics* **13**, 1168 EP – (2017). URL <http://dx.doi.org/10.1038/nphys4231>.
- <sup>8</sup> Kim, D. *et al.* Surface conduction of topological Dirac electrons in bulk insulating Bi<sub>2</sub>Se<sub>3</sub>. *Nat. Phys.* **8**, 459–463 (2012). URL <http://www.nature.com/articles/nphys2286>.
- <sup>9</sup> Hirata, M. *et al.* Observation of an anisotropic Dirac cone reshaping and ferrimagnetic spin polarization in an organic conductor. *Nat. Commun.* **7**, 12666 (2016). URL <http://www.nature.com/doi/10.1038/ncomms12666>.
- <sup>10</sup> Das Sarma, S. & Pinczuk, A. *Perspectives in quantum hall effects: Novel quantum liquids in low-dimensional semiconductor structures* (John Wiley & Sons, 2008).
- <sup>11</sup> Prange, R. & Girvin, S. *The Quantum Hall Effect* (Springer New York, 1989). URL <https://books.google.com.sg/books?id=x9pvQgAACAAJ>.
- <sup>12</sup> Ando, T. & Uemura, Y. Theory of Oscillatory g Factor in an MOS Inversion Layer under Strong Magnetic Fields. *J. Phys. Soc. Japan* **37**, 1044–1052 (1974). URL <http://journals.jps.jp/doi/10.1143/JPSJ.37.1044>.
- <sup>13</sup> Song, Y. J. *et al.* High-resolution tunnelling spectroscopy of a graphene quartet. *Nature* **467**, 185–189 (2010). URL <http://www.nature.com/doi/10.1038/nature09330>.
- <sup>14</sup> Feldman, B. E. *et al.* Observation of a nematic quantum Hall liquid on the surface of bismuth. *Science* **354**, 316–321 (2016). URL <http://www.sciencemag.org/lookup/doi/10.1126/science.aag1715>.
- <sup>15</sup> Young, A. F. *et al.* Spin and valley quantum Hall ferromagnetism in graphene. *Nat. Phys.* **8**, 550–556 (2012). URL <http://dx.doi.org/10.1038/nphys2307>.
- <sup>16</sup> Yang, K. Geometry of compressible and incompressible quantum Hall states: Application to anisotropic composite-fermion liquids. *Phys. Rev. B* **88**, 241105 (2013). URL <https://link.aps.org/doi/10.1103/PhysRevB.88.241105>. 1309.2830.
- <sup>17</sup> Balagurov, D. B. & Lozovik, Y. E. Fermi surface of composite fermions and one-particle excitations at  $\nu = \frac{1}{2}$ : effect of band-mass anisotropy. *Phys. Rev. B* **62**, 1481–1484 (2000). URL <https://link.aps.org/doi/10.1103/PhysRevB.62.1481>.
- <sup>18</sup> Balram, A. C. & Jain, J. K. Exact results for model wave functions of anisotropic composite fermions in the fractional quantum Hall effect. *Phys. Rev. B* **93**, 075121 (2016). URL <https://link.aps.org/doi/10.1103/PhysRevB.93.075121>.
- <sup>19</sup> Yang, B., Papić, Z., Rezayi, E. H., Bhatt, R. N. & Haldane, F. D. M. Band mass anisotropy and the intrinsic metric of fractional quantum Hall systems. *Phys. Rev. B* **85**, 165318 (2012). URL <https://link.aps.org/doi/10.1103/PhysRevB.85.165318>.
- <sup>20</sup> Murthy, G. *Hamiltonian Theory of Anisotropic Fractional Quantum Hall States* (2013). URL <http://arxiv.org/abs/1310.6215>. 1310.6215.

- <sup>21</sup> Kohn, W. & Luttinger, J. M. Ground-State Energy of a Many-Fermion System. *Phys. Rev.* **118**, 41–45 (1960). URL <https://link.aps.org/doi/10.1103/PhysRev.118.41>.
- <sup>22</sup> Banerjee, S., Abergel, D. S. L., Ågren, H., Aeppli, G. & Balatsky, A. V. Universal trends in interacting two-dimensional Dirac materials (2018). URL <http://arxiv.org/abs/1803.11480>. 1803.11480.
- <sup>23</sup> Giuliani, A. & Mastropietro, V. The Two-Dimensional Hubbard Model on the Honeycomb Lattice. *Commun. Math. Phys.* **293**, 301–346 (2010). URL <http://link.springer.com/10.1007/s00220-009-0910-5>. 0811.1881.
- <sup>24</sup> Trushin, M. & Schliemann, J. Pseudospin in optical and transport properties of graphene. *Phys. Rev. Lett.* **107**, 156801 (2011). URL <https://link.aps.org/doi/10.1103/PhysRevLett.107.156801>.
- <sup>25</sup> Tan, Y.-W. *et al.* Measurement of Scattering Rate and Minimum Conductivity in Graphene. *Phys. Rev. Lett.* **99**, 246803 (2007). URL <https://link.aps.org/doi/10.1103/PhysRevLett.99.246803>.
- <sup>26</sup> Das Sarma, S., Hwang, E. H., Kodiyalam, S., Pfeiffer, L. N. & West, K. W. Transport in two-dimensional modulation-doped semiconductor structures. *Phys. Rev. B* **91**, 205304 (2015). URL <https://link.aps.org/doi/10.1103/PhysRevB.91.205304>.
- <sup>27</sup> Wang, J.-R. & Liu, G.-Z. Influence of Coulomb interaction on the anisotropic Dirac cone in graphene. *Phys. Rev. B* **89**, 195404 (2014). URL <https://link.aps.org/doi/10.1103/PhysRevB.89.195404>. 1309.6999.
- <sup>28</sup> Bercx, M., Goth, F., Hofmann, J. S. & Assaad, F. F. *SciPost Phys.* **3**, 013 (2017).
- <sup>29</sup> Hohenadler, M., Parisen Toldin, F., Herbut, I. F. & Assaad, F. F. Phase diagram of the Kane-Mele-Coulomb model. *Phys. Rev. B* **90**, 085146 (2014). URL <https://link.aps.org/doi/10.1103/PhysRevB.90.085146>. 1407.2708v2.

## I. ACKNOWLEDGEMENTS

We acknowledge several discussions with João Rodrigues and Pinaki Sengupta with whom we worked closely on a separate, but related project. It is a pleasure to thank Bertrand Halperin, Jainendra Jain and Mansour Shayegan for useful suggestions. We also thank Miguel Dias Costa for assistance with the numerical parallelization, Wei Pan for providing us with the experimental data in Fig. 3, and Xingyu Gu for discussions. The work was made possible by allocation of computational resources at the CA2DM (Singapore) and the Gauss Centre for Supercomputing (SuperMUC at the Leibniz Supercomputing Center), and funding by the Singapore Ministry of Education (MOE2017-T2-1-130), Deutsche Forschungsgemeinschaft (SFB 1170 ToCoTronics, project

C01). MT acknowledges support of the CA2DM Director’s Fellowship (NRF Medium Sized Centre Programme R-723-000-001-281).

Author Contributions: SA and SDS conceived this project. HKT and FFA developed and optimized the quantum Monte Carlo codes. JNL and MT developed the analytical results under the guidance of SA and SDS. All authors discussed the results and wrote the paper.

The authors declare that they have no competing financial interests.

## METHODS

### 1. Hartree-Fock

Here, we utilize the Hartree-Fock approach to show that the renormalized anisotropy,  $\eta$ , is determined by only initial anisotropy,  $\eta_0$ , no matter how strong the interactions exactly are. To quantify the initial anisotropy we start from Hamiltonian

$$H^0 = \hbar(\hat{\sigma}_x v_x k_x + \hat{\sigma}_y v_y k_y), \quad (3)$$

where  $\hbar\mathbf{k} = (\hbar k_x, \hbar k_y)$  is the momentum in two-dimensional space, and  $\hat{\sigma}_{x,y}$  are the Pauli matrices. The velocities  $v_{x,y}$  along  $x$  and  $y$  directions define the non-interacting anisotropy,  $\eta_0 = v_x/v_y$ . The eigenvalues of  $H^0$  read  $E_{k\kappa}^0 = \kappa\hbar\sqrt{(v_x k_x)^2 + (v_y k_y)^2}$ , and the corresponding eigenstates are  $\psi_{k\kappa}^0 = \frac{1}{\sqrt{2}}e^{i\mathbf{k}\mathbf{r}}\chi_{k\kappa}$ , where  $\chi_{k\kappa} = (1, \kappa e^{i\varphi_k})^T$  with  $\kappa = \pm$  being the particle/antiparticle index. Thanks to the anisotropy  $\eta_0 \neq 0$  the chirality angle,  $\tan \varphi_k = \tan \theta_k/\eta_0$ , differs from the direction of motion,  $\tan \theta_k = k_y/k_x$ .

The mean-field interaction between fermions contains two terms which are the Hartree (direct) and Fock (exchange) terms. In the following, we will only consider the exchange interaction in the Hartree-Fock Hamiltonian, as the Hartree term is neutralised by a positive background (jellium model). Hence, the interaction term reads<sup>24</sup>

$$H^{HF} = - \sum_{\mathbf{k}'} \int \frac{d^2\mathbf{k}'}{4\pi^2} u_{|\mathbf{k}-\mathbf{k}'|} |\chi_{k'\kappa'}\rangle \langle \chi_{k'\kappa'}|, \quad (4)$$

where  $u_{|\mathbf{k}-\mathbf{k}'|} = 2\pi e^2/\epsilon|\mathbf{k}-\mathbf{k}'|$  is the two-dimensional Fourier transform for Coulomb potential with  $\epsilon$  being the dielectric constant. We employ the non-interacting plane-wave solution to diagonalize the total Hamiltonian  $H = H^0 + H^{HF}$ . Near half-filling, only antiparticle states contribute to the exchange term. Since the antiparticle band does not have a bottom in our model we assume some momentum cutoff  $\Lambda$  to make the integral over occupied states converging. Hence, the Hartree-Fock energy results in equation (1) with the interband chirality factor explicitly given by

$$\begin{aligned} & \sin^2\left(\frac{\varphi_k - \varphi'_k}{2}\right) \\ &= \frac{1}{2} \left( 1 - \frac{\eta_0^2 \cos \theta_k \cos \theta_{k'} + \sin \theta_k \sin \theta_{k'}}{\sqrt{\eta_0^2 \cos^2 \theta_k + \sin^2 \theta_k} \sqrt{\eta_0^2 \cos^2 \theta'_{k'} + \sin^2 \theta'_{k'}}} \right). \end{aligned} \quad (5)$$

Thanks to the chirality factor and the vast antiparticle fermion sea the interaction energy (1) does not vanish even at the Dirac point, where the Fermi surface shrinks to zero. This mechanism maintains strong interactions between Dirac fermions no matter how high the fermion concentration is. The renormalized velocity components  $v_{x,y}^{HF} = \frac{1}{\hbar} \frac{\partial E^{HF}(\mathbf{k})}{\partial k_{x,y}}$  can be written as

$$\begin{aligned} \frac{v_x^{HF}}{v} &= \frac{r_s}{\pi} \ln\left(\frac{\Lambda}{k}\right) \frac{\eta_0}{\eta_0^2 - 1} \\ &\quad \times [\text{E}(1 - \eta_0^2) - \text{K}(1 - \eta_0^2)], \end{aligned} \quad (6a)$$

$$\begin{aligned} \frac{v_y^{HF}}{v} &= \frac{r_s}{\pi} \ln\left(\frac{\Lambda}{k}\right) \frac{\eta_0}{\eta_0^2 - 1} \\ &\quad \times \left[ \text{K}\left(1 - \frac{1}{\eta_0^2}\right) - \text{E}\left(1 - \frac{1}{\eta_0^2}\right) \right], \end{aligned} \quad (6b)$$

where  $r_s = e^2/(\epsilon\hbar v)$ ,  $v = \sqrt{v_x v_y}$ , and  $\text{K}(z)$  and  $\text{E}(z)$  are the complete elliptic integrals of the first and second kind respectively. Note that  $v_{x,y}^{HF}$  diverge logarithmically at half-filling, hence,  $v_{x,y}^{HF} \gg v_{x,y}$ . The interacting anisotropy  $\eta$  would then be the anisotropy of the Hartree-Fock velocity given by the ratio of  $\eta = v_x^{HF}/v_y^{HF}$ , see equation (1).

It is instructive to compare this result with the Hartree-Fock model for anisotropic Schrödinger fermions that can be modeled by the non-interacting Hamiltonian

$$H^0 = \frac{\hbar^2 k_x^2}{2m_x} + \frac{\hbar^2 k_y^2}{2m_y}, \quad (7)$$

where  $m_{x,y}$  is the anisotropic effective mass. The anisotropy of the Fermi surface is characterized in the same way as for Dirac fermions, i.e.

$$\eta_0 = \frac{|\mathbf{k}_{\parallel y}|_{E=E_F^0}}{|\mathbf{k}_{\parallel x}|_{E=E_F^0}} = \underbrace{\frac{v_x}{v_y}}_{\text{Dirac}} = \underbrace{\sqrt{\frac{m_y}{m_x}}}_{\text{Schrödinger}}. \quad (8)$$

The Hartree-Fock exchange energy is

$$E^{HF}(\mathbf{k}) = - \int_{E_0(\mathbf{k}') < E_F^0} \frac{d^2\mathbf{k}'}{(2\pi)^2} \frac{2\pi e^2}{\epsilon|\mathbf{k}-\mathbf{k}'|}. \quad (9)$$

There is no antiparticle band, no chirality factor, and no need of momentum cut-off here. The anisotropy of the Hartree-Fock spectrum varies when we move up the Fermi energy level. The interacting anisotropy is determined at the Fermi level of the interacting fermions by keeping their density fixed. The result is plotted in Fig. 4b. As shown there, the Fermi surface anisotropy behaves in

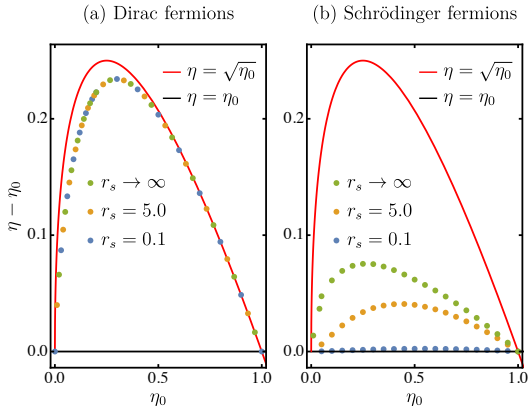


FIG. 4. Change in Fermi surface anisotropy within Hartree-Fock theory for electron-electron interactions for (a) 2D Dirac fermions and (b) 2D Schrödinger fermions. Dirac fermions with long-range interactions follow closely the universal square root behavior  $\eta = \sqrt{\eta_0}$  (red line) independent of interaction strength  $r_s$ , whereas for the parabolic dispersion, the anisotropy renormalization makes the system more isotropic in a non-universal way. The renormalized anisotropy for the parabolic dispersion is closer to the non-interacting value, and never approaches the  $\sqrt{\eta_0}$  even for strong interactions.

different ways depending whether Dirac or Schrödinger fermions are considered. For Dirac fermions, the interacting anisotropy is not sensitive to the interaction strength and follows a square-root trend. For Schrödinger fermions, the interacting anisotropy depends on  $r_s$ , which measures the relative strength between the Coulomb energy and the Fermi energy. We see that when  $r_s$  is increased, demonstrating transition from non-interacting to strongly interacting limit, the interacting anisotropy is bounded by the green data points obtained in the limit  $E^{HF} \gg E^0$ . Hence, the  $\sqrt{\eta_0}$ -like anisotropy dependence is not possible for Schrödinger fermions at any interaction strength leaving Dirac fermions unique in this sense.

It is interesting to note that the particle-antiparticle asymmetry does not influence the universal behaviour of  $\eta$ . Indeed, any term proportional to the  $2 \times 2$  identity matrix added into the non-interacting Hamiltonian (3) is not able to alter the chirality factor even though it can change the dispersion and break the electron-hole symmetry. Since the universality of equation (2) is due to the chirality factor, it remains unaltered as well.

## 2. Perturbation Theory

Since the Coulomb interaction in our considerations is instantaneous, the first order perturbation theory is equivalent to the Hartree-Fock approximation. The correction to the non-interacting spectrum  $E_0(\mathbf{k})$ , here it is named self-energy in the context of perturbation theory, is given by the one loop diagram

$$\Sigma(\mathbf{k}) = \int \frac{d\omega d^2\mathbf{q}}{(2\pi)^3} \frac{2\pi e^2}{\epsilon |\mathbf{k} - \mathbf{q}|} G_0(\omega, \mathbf{q}), \quad (10)$$

where the non-interacting Green's function is given by  $G_0(\omega, \mathbf{q}) = (i\omega - \xi_{\mathbf{q}})^{-1}$  and  $\xi_{\mathbf{q}} = E_0(\mathbf{q}) - \mu$  is the non-interacting energy measured from the chemical potential, that is equivalent to the Fermi energy at zero temperature. Since the Coulomb interaction has no frequency dependence, the frequency integration is only performed on the non-interacting Green's function. The usual frequency summation of the non-interacting Green's function gives the Fermi-Dirac distribution  $n_F(\xi_{\mathbf{q}}) = [\exp(\xi_{\mathbf{q}}/k_B T) + 1]^{-1}$ . At zero temperature, the Fermi-Dirac distribution resolves to a step function, which restricts the momentum integration to within the Fermi surface. Thus, we see that the self-energy

$$\Sigma(\mathbf{k}) = - \int_{E_0(\mathbf{q}) < E_F^0} \frac{d^2\mathbf{q}}{(2\pi)^2} \frac{2\pi e^2}{\epsilon |\mathbf{k} - \mathbf{q}|} \quad (11)$$

is equivalent to the Hartree-Fock approximation given in Eqn. (9). For the Dirac model, one may choose to go to the eigenbasis of the non-interacting Green's function, where the self-energy would be evaluated to the similar expression as in Schrödinger system, except that the unitary transformation gives rise to an additional chirality factor. With the inclusion of the chirality factor, the self-energy within the first order perturbation theory is equivalent to the Hartree-Fock exchange energy for the Dirac model as in Eqn. (1).

To show the robustness of the results against the choice of basis, here we present also the first order perturbation theory in the sub-lattice basis. In this basis, the non-interacting Green's function in Eqn. (10) is  $G_0(\omega, \mathbf{k}) = (-i\omega_k \sigma_0 + v_x \sigma_x k_x + v_y \sigma_y k_y)^{-1}$ , where  $\sigma_{x,y}$  are the Pauli matrices, and  $\sigma_0$  is the identity matrix. Upon frequency integration, the self-energy is evaluated to

$$\Sigma(\mathbf{k}) = \frac{e^2}{4\pi\epsilon} \times \int \frac{d^2\mathbf{q}}{\sqrt{k^2 + q^2 - 2kq \cos(\theta_k - \theta_q)}} \frac{\eta_0 \sigma_x q_x + \sigma_y q_y}{\sqrt{\eta_0^2 q_x^2 + q_y^2}}. \quad (12)$$

The corresponding velocity components may be evaluated in a similar way to that described in the previous subsection and give the same results as in Eqn. (6).

In the case where the Dirac fermions are interacting with contact interactions, there is no contribution to the self-energy within the first order perturbation theory. This can be seen in the sub-lattice basis where the contact interaction acts on the electrons in the same sub-lattice, but after the integration over the frequency  $\omega$ , the Green's function propagates the electrons to the other sub-lattice. Thus the product of the matrix elements vanishes for both the diagonal and off-diagonal terms, resulting in no contribution to the self-energy. We understand that this is due to Pauli exclusion principle: the Hubbard term only connects electrons with opposite spins, but within first order perturbation theory, we consider only the self-interaction of the particle. Since the particle does not change the spin during the propagation, we conclude that the contact interaction has no effect, and as a result, the interacting anisotropy  $\eta$  remains the same as the non-interacting anisotropy  $\eta_0$  for a system with only contact interactions.

Going beyond first order perturbation theory, we may analyze the problem within the random phase approximation (RPA). For the Dirac fermions, renormalization group study considering the RPA contributions shows that the Fermi velocity anisotropy flows to the isotropic limit at low energy scale<sup>27</sup>. However, in a perturbative approach, the interacting system, though is less anisotropic than the non-interacting one, is not totally isotropic as predicted by the renormalization group flow. Expanding the perturbative results for small coupling constant  $r_s$ , we find

$$\eta = \frac{E(1 - \eta_0^2) - K(1 - \eta_0^2)}{K(1 - \eta_0^{-2}) - E(1 - \eta_0^{-2})} + \frac{2\pi\eta_0^2 - 1}{3} \frac{\eta_0^{3/2}}{\eta_0^2} \frac{E(1 - \eta_0^{-2}) - K(1 - \eta_0^2)}{[E(1 - \eta_0^{-2}) - K(1 - \eta_0^2)]^2} r_s + \mathcal{O}(r_s^2). \quad (13)$$

To extract the single-particle interacting energy from the PQMC, we compute the zero-temperature single-

To leading order, this result is consistent with the Hartree-Fock result in Eqn. (2).

### 3. Quantum Monte Carlo

In addition to the perturbative theories, we employ projective quantum Monte Carlo (PQMC)<sup>28</sup> that has recently been adapted to include the long-range Coulomb interaction. We study interacting fermions on a honeycomb lattice described by the Hamiltonian

$$\hat{H} = -t \sum_{\langle ij \rangle, \sigma} (\hat{c}_{i\sigma}^\dagger \hat{c}_{j\sigma} + \text{h.c.}) + \frac{1}{2} \sum_{i,j} (\hat{n}_i - 1) \mathcal{V}_{ij} (\hat{n}_j - 1) \quad (14)$$

where h.c. is the Hermitian conjugate,  $t$  is the tight-binding hopping, the second-quantized operator  $\hat{c}_{i\sigma}^\dagger$  ( $\hat{c}_{i\sigma}$ ) creates (annihilates) an electron of spin  $\sigma = \uparrow\downarrow$  at position  $\mathbf{r}_i$ , and  $\hat{n}_i = \sum_\sigma \hat{c}_{i\sigma}^\dagger \hat{c}_{i\sigma}$  gives the electron density at position  $\mathbf{r}_i$ . The interaction  $\mathcal{V}_{ij}$  consists of a short-range part acting between electrons on the same site with different spins,  $\mathcal{V}_{ii} = U$ , and a long-range part depending on the distance between the electrons  $r_{ij} = 2a|\mathbf{r}_i - \mathbf{r}_j|/3$  as  $\mathcal{V}_{ij} = a_0/r_{ij}$ , where  $a$  is the lattice constant.

In the PQMC, we choose the non-interacting ground state as our trial wavefunction  $\Psi_T$ , and compute the expectation values of an observable by projecting out the interacting ground state from the trial wave function

$$\langle \hat{O} \rangle = \frac{\langle \Phi_0 | \hat{O} | \Phi_0 \rangle}{\langle \Phi_0 | \Phi_0 \rangle} = \lim_{\Theta \rightarrow \infty} \frac{\langle \Psi_T | e^{-\Theta \hat{H}/2} \hat{O} e^{-\Theta \hat{H}/2} | \Psi_T \rangle}{\langle \Psi_T | e^{-\Theta \hat{H}} | \Psi_T \rangle}, \quad (15)$$

where  $\Theta$  is set to  $40/t$ . The key step in the PQMC is to perform Hubbard-Stratonovich transformation at each imaginary time slice to decouple a quartic fermionic term down to a bilinear one, at the cost of introducing an auxiliary field<sup>29</sup>

$$\exp \left( \delta\tau \sum_{i \leq j} V_{ij} (n_i - 1)(n_j - 1) \right) = \int dA \exp \left( -\delta\tau/4 \sum_{x,y} A_x (V^{-1})_{xy} A_y + i \sum_x A_x (n_x - 1) \right). \quad (16)$$

particle Green's function

$$G_k(\tau) \equiv \left\langle \Phi_0^{(N)} \left| \hat{c}_k^\dagger(\tau) \hat{c}_k(0) \right| \Phi_0^{(N)} \right\rangle. \quad (17)$$

The Green function can be rewritten as

$$G_k(\tau) = \sum_n \left| \left\langle \Phi_0^{(N)} \left| \hat{c}_k^\dagger \left| \chi_n^{(N-1)} \right. \right. \right\rangle \right|^2 e^{-(E_n^{(N-1)} - E_0^{(N)})\tau}, \quad (18)$$

where  $\left| \chi_n^{(N-1)} \right\rangle$  are the eigenstates in the  $N - 1$  particle number sector with eigen energy  $E_n^{(N-1)}$ . In the limit of large imaginary times,  $\tau \rightarrow \infty$ , the Green's function becomes

$$G_k(\tau \rightarrow \infty) \rightarrow Z_k e^{-(E_0^{(N-1)} - E_0^{(N)})\tau}, \quad (19)$$

where  $Z_k \equiv \left| \left\langle \Phi_0^{(N)} \left| \hat{c}_k^\dagger \left| \chi_0^{(N-1)} \right. \right. \right\rangle \right|^2$  is the quasiparticle weight of the lowest-lying single particle excitation at momentum  $\mathbf{k}$ . The single-particle interacting energy at momentum  $\mathbf{k}$  is then obtained by fitting an exponential decay to the imaginary time Green's function  $G_k$  at large  $\tau$ .

We simulate systems with  $L = 6, 9, 12, 15, 18$  and 24 unit cells along each directions, amounting to a

total of  $2L^2$  lattice sites. Since these systems with different sizes do not share the same reciprocal lattice sites, we interpolate our results to a common set of momenta. To obtain the energy renormalization  $E - E_0$  in the thermodynamic limit, we extrapolate the results obtained from different system sizes to  $L \rightarrow \infty$  using a fit to the form  $a + b/L^2$ . The results along the two crystalline directions  $K - K'$  and  $K - \Gamma$  are plotted in Fig. 2.

#### 4. Lattice Perturbation Theory

While PQMC is non-perturbative and numerically exact, it is limited by the size of the system. To complement the PQMC, we employ perturbation theory to the fermions on honeycomb lattice. Unlike the continuum Dirac model, here we retain the lattice structure, and hence the anisotropy between the  $K - K'$  and  $K - \Gamma$  directions. Within the first order, the self-energy is given as the convolution of the non-interacting Green's function  $G_0(\omega, \mathbf{k})$  and the interaction  $\mathcal{V}(\mathbf{k})$  over the momentum space,

$$\Sigma_{\mu\nu}(\mathbf{q}) = \frac{1}{2L^4} \int \frac{d\omega}{2\pi} \sum_{\mathbf{k}} [\mathcal{V}_{\mu\nu}(\mathbf{k}) G_0^{\mu\nu}(\omega, \mathbf{q} + \mathbf{k}) + \mathcal{V}_{\nu\mu}(\mathbf{k}) G_0^{\mu\nu}(\omega, \mathbf{q} - \mathbf{k})], \quad (20)$$

where  $\mu, \nu$  are the matrix indices denoting the sub-lattices. The non-interacting Green's function is expressed in the sub-lattice basis as

$$G_0^{-1}(\omega, \mathbf{k}) = \begin{pmatrix} -i\omega & \sum_i e^{-i\mathbf{k}\cdot\boldsymbol{\delta}_i} \\ \sum_i e^{i\mathbf{k}\cdot\boldsymbol{\delta}_i} & -i\omega \end{pmatrix}, \quad (21)$$

where  $\boldsymbol{\delta}_1 = (0, 1/\sqrt{3})a$ ,  $\boldsymbol{\delta}_2 = (-1/2, 1/2\sqrt{3})a$  and  $\boldsymbol{\delta}_3 = (1/2, 1/2\sqrt{3})a$  are the position of the nearest neighbours in the real space. On the other hand, the interaction in the sub-lattice basis is given as

$$\mathcal{V}(\mathbf{k}) = \sum_{\mathbf{x}, \mathbf{y}} \begin{pmatrix} \mathcal{V}(|\mathbf{y} - \mathbf{x}|) & \mathcal{V}(|\mathbf{y} - \mathbf{x} + \boldsymbol{\delta}_1|) \\ \mathcal{V}(|\mathbf{y} - \mathbf{x} - \boldsymbol{\delta}_1|) & \mathcal{V}(|\mathbf{y} - \mathbf{x}|) \end{pmatrix} e^{i\mathbf{k}\cdot(\mathbf{y} - \mathbf{x})}, \quad (22)$$

where  $\mathcal{V}(r) = e^2/\epsilon r$  is the Coulomb interaction. We numerically compute the self-energy  $\Sigma(\mathbf{q})$  for system size of  $1500 \times 1500$  unit cells and interpolate our results to obtain a continuous spectrum for the self-energy. The interacting theory anisotropy  $\eta$  is then calculated by considering

the equi-energy contour of the self-energy  $\Sigma(\mathbf{q})$ . We see in Fig. 2b that both the quantum Monte Carlo results and the lattice perturbation theory with long-range interactions agree with the universal square-root behavior.

#### 5. Boltzmann Transport

In the absence of magnetic field, the electrons behave as Schrödinger fermions. The linear dependence of mobility on electron density<sup>7</sup> indicates that the impurity scattering is Coulombic. Assuming that disorder is due to  $Z = 1$  charged impurities described by the bare Coulomb potential  $V(r) = e^2/(\epsilon r)$ , the relaxation time is given as

$$\frac{1}{\tau(\varepsilon_k)} = \int \frac{d^2\mathbf{k}'}{(2\pi)^2} w_{\mathbf{k}\mathbf{k}'} (1 - \cos\theta'), \quad (23)$$

where the scattering probability due to impurities of concentration  $n_i$  from momentum  $\mathbf{k}$  to momentum  $\mathbf{k}'$  is

$$w_{\mathbf{k}\mathbf{k}'} = \frac{2\pi}{\hbar} n_i \left( \frac{2\pi e^2}{\epsilon} \right)^2 \frac{f_{\mathbf{k}\mathbf{k}'} \delta(\varepsilon_k - \varepsilon_{k'})}{k'^2 + k^2 - 2kk' \cos(\theta' - \theta)}. \quad (24)$$

According to Boltzmann transport theory, the conductivity is related to the relaxation time through the equation

$$\sigma = 2e^2 \int \frac{d^2\mathbf{k}}{(2\pi)^2} (v \cos \theta)^2 \tau(\varepsilon_k) \delta(\varepsilon_k - E_F). \quad (25)$$

For Schrödinger fermions  $\varepsilon_k = \hbar^2 k^2 / (2m)$ ,  $v = \hbar k / m$  and the chirality factor  $f_{\mathbf{k}\mathbf{k}'} = 1$ , we find

$$\sigma_S = \frac{e^2}{h} \frac{4n}{\pi r_s^2 n_i}, \quad (26)$$

where  $n = k_F^2 / (2\pi)$  is the density with the spin degeneracy included, and  $r_s = e^2 / (\epsilon \hbar v)$  depends on  $n$  via  $v$ . Using the parameters relevant to GaAs ( $\epsilon = 12.9$ ,  $m = 0.063m_e$ ), we fit the experimental conductivity at  $B = 0$  for the impurity concentration to find  $n_i = 1.9 \times 10^7 \text{ cm}^{-2}$  for sample A and  $n_i = 9.6 \times 10^6 \text{ cm}^{-2}$  for sample B.

In the case of Dirac fermions with the linear dispersion  $\varepsilon_k = \hbar v k$  and intraband chirality factor  $f_{\mathbf{k}\mathbf{k}'} = \cos^2(\frac{\theta' - \theta}{2})$ , the conductivity obtained from Eqn. (23)–(25) is  $\sigma_D = \sigma_S / 2$  where  $r_s$  is the density independent fine-structure constant. Using the above impurity concentration obtained from fitting the experimental data at  $B = 0$ , we can now fit the conductivity to the experimental data at  $\nu = 1/2$  to obtain the composite Fermi liquid Dirac velocity. We find  $v = 1.8 \times 10^6 \text{ cm/s}$  corresponding to  $r_s = 9.6$ . The fits are plotted in Fig. 3.

## DATA AVAILABILITY

The quantum Monte Carlo data presented in this article can be reproduced using the Algorithms for Lattice Fermions (ALF) open-source general implementation of the finite temperature auxiliary field quantum Monte Carlo available at <https://alf.physik.uni-wuerzburg.de> and documented in Ref. 28. All other data that support these results are available from the corresponding author upon request.